Geology of El Misti volcano near the city of Arequipa, Peru

Jean-Claude Thouret, Anthony Finizola, Michel Fornari, Annick Legeley-Padovani, Jaime Suni, Manfred Frechen

Geology of El Misti volcano near the city of Arequipa, Peru

Jean-Claude Thouret*
Anthony Finizola
UMR 6524-CNRS Laboratoire Magmas et Volcans, and *Institut de Recherche pour le Développement, Université Blaise-Pascal, 5 rue Kessler, 63038 Clermont-Ferrand cedex, France*

Michel Fornari
IRD, UMR 6526-CNRS "Géosciences Azur," Faculté des Sciences, Université de Nice, Parc Valrose, 06108 Nice cedex 02, France

Annick Legeley-Padovani
Laboratoire de Géophysique Interne, Centre IRD Ile-de-France, 34 rue Henri-Varagnat, 93143 Bondy cedex, France

Jaime Suni
Instituto Geofísico del Perú, Oficin Regional, Urbanización La Marina B19, Cayma, and *Universidad Nacional San Agustín, Arequipa, Perú*

Manfred Frechen
Centre for Environmental Change and Quaternary Research, GEMRU, Francis Close Hall, Swindon Road, Cheltenham GL50 4AZ, UK

ABSTRACT

Approximately 750 000 people live at risk in the city of Arequipa, whose center lies 17 km from the summit (5820 masl [meters above sea level]) of the active El Misti volcano. The composite edific comprises a stratovolcano designated Misti 1 (ca. 833–112 ka), partially overlapped by two stratocones designated Misti 2 and Misti 3 (112 ka and younger), and a summit cone Misti 4 (11 ka and younger).

Eight groups of lava flow and pyroclastic deposits indicate the following volcanic history. (1) Three cones have been built up since ca. 112 ka at an average eruptive rate of 0.63 km³/k.y. (2) Several episodes of growth and destruction of andesitic and dacitic domes triggered dome-collapse avalanches and block-and-ash-flows Deposition of these flow alternated with explosive events, which produced pyroclastic-flo deposits and tephra-fall and surge deposits. (3) Nonwelded, dacitic ignimbrites may reflec the formation of a 6 × 5 km incremental caldera collapse on Misti 2 (ca. 50 000 and 40 000 yr B.P.) and a 2 × 1.5 km summit caldera on Misti 3 (ca. 13 700 to 11 300 yr B.P.). (4) Tens of pyroclastic flow and at least 20 tephra falls were produced by Vulcanian and sub-Plinian eruptions since ca. 50 ka. On average, ash falls have occurred every 500 to 1500 yr, and pumice falls, every 2000 to 4000 yr. (5) Misti erupted relatively homogeneous andesites and dacites with a few rhyolites, but Misti 4 reveals a distinct mineral suite. Less evolved andesites prevail in scoriaceous products of group 4–1 including historical ash falls. Scoriae of Misti 4 and the ca. 2300–2050 yr B.P. banded pumice commonly show heterogeneous textures of andesite and rhyolite composition. This heterogeneity may reflec changes in physical conditions and magma mixing in the reservoir. (6) Deposits emplaced during the Vulcanian A.D. 1440–1470 event and the sub-Plinian eruption(s) at ca. 2050 yr B.P. are portrayed on one map. The extent and volume of these deposits indicate that future eruptions of El Misti, even if moderate in magnitude, will entail considerable hazards to the densely populated area of Arequipa.

INTRODUCTION

El Misti is one of the seven potentially active volcanoes of the Central Andean volcanic zone of south Peru (de Silva and Francis, 1991). The Pleistocene volcanic range parallels the N120°-trending boundary of the Western Cordillera, oblique to the N80° convergence of the Nazca plate along the Peruvian margin (Fig. 1). Straddling the south slope of the Cordillera Occidental and the north edge of the Arequipa depression, El Misti is the most recently active edific of a cluster of Pleistocene volcanoes, which includes the dormant Chachani compound volcano, 15 km to the northwest, and the extinct Pichu Pichu compound volcano, 20 km to the southeast (Fig. 1; Thouret et al., 1995; Thouret, 1999b). El Misti lies within a complex extensional and strike-slip tectonic setting of four groups of faults: the active, west-northwest–trending, normal-slip, en echelon Huanca fault, dipping southwest with a moderate left-lateral strike-slip component, which offsets the probably inactive north-, northeast-, and north-northwest–trending normal- and strike-slip faults. The northeast-trending faults and the inherited north-trending compressive faults have guided the formation of the 1-km-deep Río Chili canyon that drains the Cordillera Occidental toward the Arequipa tectonic basin at 2300 masl.

Eruptive activity at El Misti represents an impending threat for the 750 000 inhabitants of Arequipa, Peru's second-largest city, cen-

*E-mail: thouret@opgc.univ-bpclermont.fr.

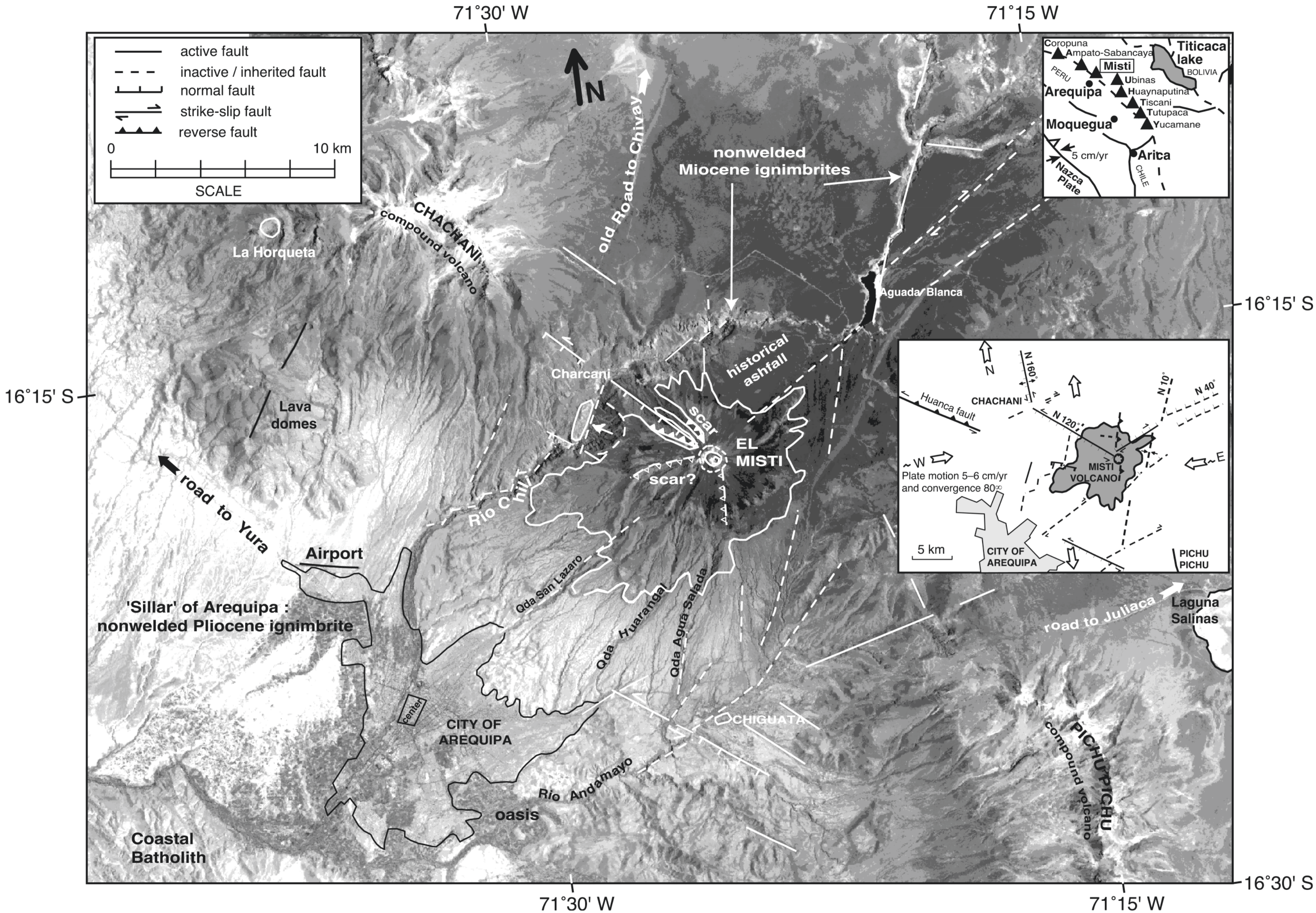

Figure 1. Landsat satellite scene showing the tectonic setting of the Cordillera Occidental, the Arequipa depression, and three volcanoes: the active Holocene El Misti volcano (a composite edifice) the dormant Chachani–La Horqueta compound volcano, and the extinct Pichu Pichu compound massif. Qda—Quebrada (= ravine). Inset top right: Location of the Pleistocene volcanoes in the Central Andean volcanic zone of southern Peru with respect to the Peru-Chile trench (line with open triangular "tooth" on upper plate). Inset right: Main tectonic features.

tered at 2300 masl and situated only 17 km to the southwest and 3.5 km lower in elevation than the volcano summit. Arequipa was founded in 1540 on the bank of the Río Chili at an oasis but remained small until 1940 (when its population was 86 000). The population of Arequipa was 677 000 in 1995 and since then has grown annually by as much as 5.5% (INEI-ORSTOM, 1998). Settlements now occupy two-thirds of the oasis area and the volcaniclastic fans that Quebradas (= ravines) San Lazaro and Huarangal have formed on the southwest ring plain of El Misti (Fig. 2A). Since 1980, the city has spread out upstream within 13 km of the summit near the quebradas that drain the southwest flank of the volcano, as well as west and east of the oasis. At least 220 000 people live at risk from pyroclastic flows lahars, and flood on the fans and near quebradas. Of these, 50 000 people live in suburbs along the Quebradas Huarangal and San Lazaro, and 170 000 people live in the northeastern neighborhoods and in the town of Chiguata, 11 km south of the summit (Fig. 1).

Our geologic study was prompted by a joint research program (1995–1999) led by Institut de Recherche pour le Développement de France Hand Instituto Geofísico del Perú. Before our study, work on Ph.D. theses had addressed the stratigraphy of the Misti volcanic deposits (Macedo, 1994; Legros, 1998; Suni, 1999). Petrologic data were obtained by Lefèvre (1979), Legendre (1999), and one K-Ar date on a Misti lava flo was published by Kaneoka and Guevara (1984). The aim of this paper therefore is to determine (1) the geologic and volcanic setting of the Misti volcano, (2) the stratigraphy and chronology of the recent deposits of El Misti, based on geologic mapping and stratigraphic sections, and (3) the extent of the most recent tephra that has been erupted toward Arequipa.

STRATIGRAPHY AND ERUPTION HISTORY

El Misti comprises two edifices an eroded stratovolcano termed "Misti 1" partly overlapped by pristine stratocone edifice termed "Misti 2," "Misti 3," and "Misti 4" (Figs. 2A and 3–5). The edifice have been built on top of "pre-Misti" volcaniclastic sediment (VS0 in Fig. 4) that unconformably overlies nonwelded rhyodacitic ignimbrites (Figs. 2B and 3–5), inaccurately termed "sillars" (Barker, 1996). The ignimbrites, which are ≥300 m in thickness in the Río Chili canyon (Fig. 2B; NI0 in Fig. 4) were emplaced as early as ca. 13.8 to 13.1 Ma (^{40}Ar-^{39}Ar, Fig. 6, col. B; Table 1; see also Data Repository[1]); the youngest "white sillar" of Arequipa yielded a fission track age of ca. 2.4 Ma (Vatin-Pérignon et al., 1996).

Pre-Misti and Misti 1 Stratovolcano

Misti 1 (ca. 833 to >112 ka; Figs. 3–6) consists of andesite lava flow as long as 9 km interbedded with thin volcaniclastic sediment and nonwelded ignimbrites, totaling ≥400 m in thickness. Above the Neogene ignimbrites, one lava flo at the base of Misti 1 was dated at ca. 833 ka (Fig. 2A; LF1 in Fig. 4; Fig. 6, col. B; Table 1; Data Repository).

Subdued, Distal Debris-Avalanche Deposit

El Misti shows no failure scar, except on the eroded west-northwest flan and possibly on the south flank however, two debris-avalanche deposits are found around El Misti (Figs. 2A, 3, and 4). The older deposit appears as DA0 in Figure 4.

To the southeast as far as 25 km away from the Misti summit, distal debris-avalanche deposits form hummocks ≥100 m thick in an ~100 km^2 area of the Arequipa basin and onto the west flan of the extinct Pichu Pichu volcano. The mixed and debris-block facies (after Glicken, 1991) of the hummocks are lithologically diverse and hydrothermally altered (Fig. 2C). The subdued hummocky topography, higher in elevation in the area of Río Andamayo (Fig. 4), has been interpreted to be the result of flan failures of the extinct Pichu Pichu volcano (Legros, 1998). However, major element, trace element, and rare earth element compositions of lava clasts (Legendre, 1999) from the debris-avalanche deposits are similar both east and south of Misti but differ from the lavas of Pichu Pichu. The Nb/La, Th/La, and Yb/La ratios of most of the debris-avalanche clasts (Legendre, 1999) are similar to the ratios in Misti's lavas, and this result points toward El Misti as the probable source. However, we do not know whether the flan failure, which produced the subdued, distal debris-avalanche deposits, occurred on a pre-Misti volcano or on Misti 1.

Proximal, Nonweathered Debris-Avalanche Deposit

The second debris-avalanche deposit at least 50 m thick found around El Misti covers the south and southwest flank (an ~40 km^2 area) as far as 12 km to the southwest (Quebrada San Lazaro) and south (Quebrada Mariano Melgar) of the summit. The deposit forms flat-toppe terrain in which nonweathered, dacitic and rhyolitic debris-block facies fille topographic lows that channeled the avalanches on the south flank Deposits with similar debris-block facies and composition crop out also on the steep northwest flan of Misti in the Río Chili canyon (DA1 in Fig. 4). These deposits overlie nonwelded dacitic ignimbrites of Misti 1 (El Chilcal, Fig. 3) and are overlain by the ca. 112 ka lava flow of Misti 2. Thus, a flan failure on Misti 1 may have triggered the proximal, nonweathered debris-block facies avalanche.

Misti 2–4 Stratocones Formed Since ca. 112 ka

The Misti 2, 3, and 4 stratocones (112 ka and younger) consist of stubby lava flow and pyroclastic debris as thick as 2.2 km (Fig. 5). Pyroclastic debris shed by the cones moved downslope 10 to 25 km away from the summit; the debris mantled the slopes of El Misti and formed an extensive volcaniclastic ring plain with an area of ~200 km^2. The deposits include two fans (Quebradas San Lazaro and Huarangal, Figs. 2A and 3) upon which the city of Arequipa has grown. Composite stratigraphic sections show seven groups of lava and pyroclastic-flo , -fall, and -surge deposits. The sections are amplifie by fiel mapping, lithologic and petrologic study, and forty ^{40}Ar-^{39}Ar, thermoluminescence (TL), and ^{14}C dates (Fig. 6, col. A; Tables 1 and 2; Data Repository). The groups record the growth and destruction of Misti 2–4 during since 112 ka.

Misti 2 Stratocone

Group 2–1, ca. 112–70 ka. The stratigraphically basal group consists of stubby lava flow and block-lava flow of domes that form steep fronts and a break in slope at the base of Misti 2 (3000–3800 masl) toward the south, southwest, east, and northeast (Fig. 3; LF2 in Fig. 4; Fig. 6, col. B; Table 1). Extrusive activity occurred between ca. 110 and 70 ka (Fig. 6). Group 2–1 also includes block-and-ash flow and scoriaceous and pumiceous pyroclastic-flo deposits. The succession is interbedded with lava flows which have built up Misti 2 as high as 4000 to 4500 masl (Figs. 4 and 5).

Group 2–2, ca. 70–50(?) ka. Group 2–2 deposits are andesite and dacite blocks 10 to

GSA Data Repository item 2001135, description of Ar/Ar and TL dates and of geochemistry and minerals in lavas and tephras, is available on the Web at http://www.geosociety.org/pubs/ft2001.htm. Requests may also be sent to editing@geosociety.org.

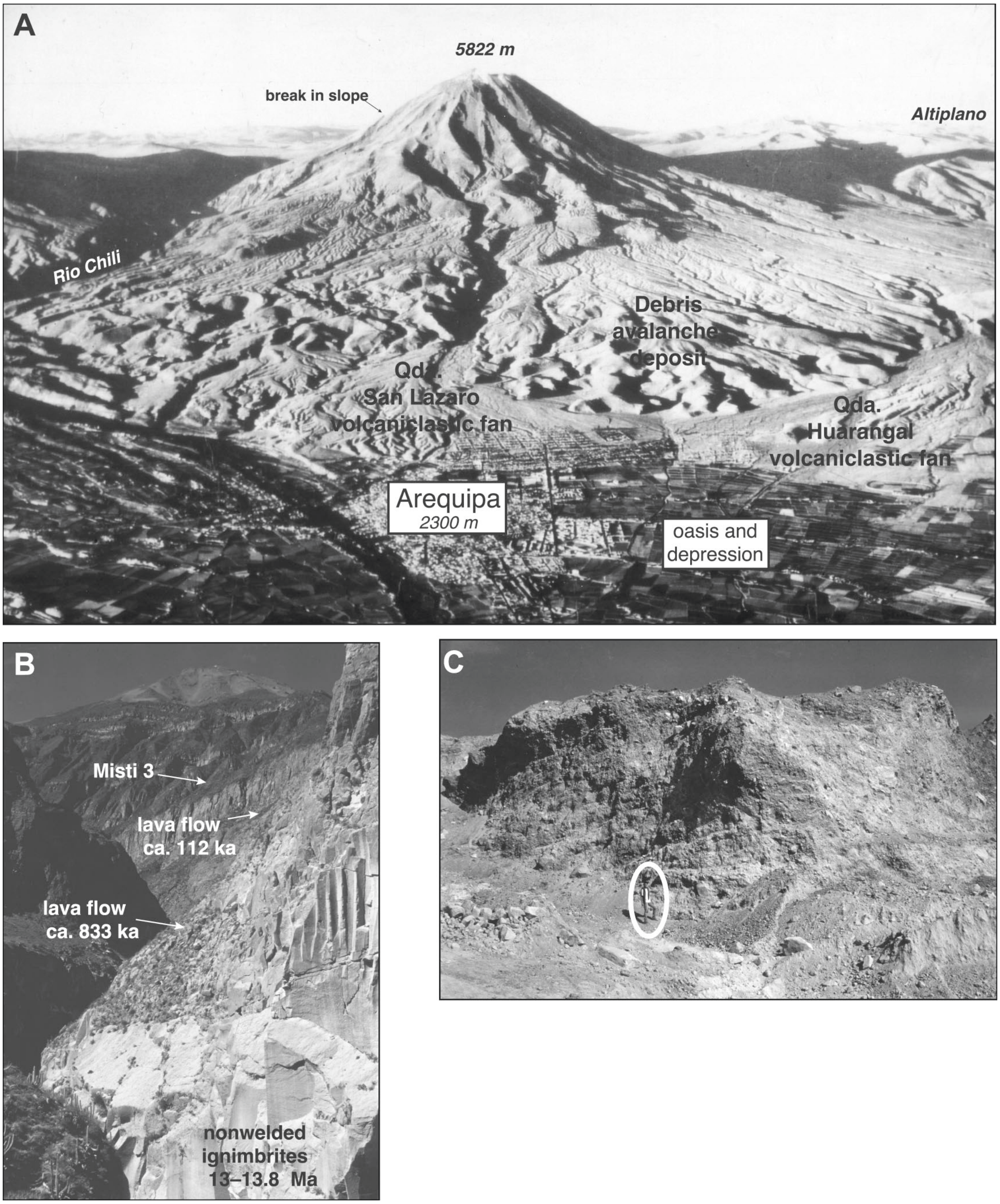

Figure 2. (A) El Misti stratovolcano looking northeast over the depression and town of Arequipa in 1940 (courtesy of I. Parodi). Break in slope at ~4400 masl coincides with a structural boundary. (B) "Pre-Misti" nonwelded ignimbrites and lava flow of Misti 1, in the 1-km-deep Río Chili canyon, overlain by the 2.2-km-thick cones of Misti 2, Misti 3 (shown), and Misti 4. (C) Mixed and debris-block facies of a debris avalanche 14 km south of the Misti summit (road to Chiguata).

20 m thick, found as far as 11 km down valley from the vent in the Quebradas Agua Salada, Pastores, and Huarangal (DC2 in Fig. 4; Fig. 7, A and B; and Fig. 8, cols. 1–3). The matrix-poor deposit containing dome blocks indicates collapse of voluminous domes that had grown on the firs stratocone at 3800–4500 masl. Prismatically jointed blocks indicate that the dome-collapse deposits were emplaced hot.

Interbedded with group 2–2 andesite (as well as with group 2–3 rocks, described next), greenish scoriaceous and pumiceous-flo and -fall deposits mantle the southeast flan of Chachani volcano and parts of the southwest flan of Misti to depths of 10 m (Fig. 7B and Fig. 8, cols. 2 and 6). The dark mafi andesite (53%–55% SiO_2) scoriaceous lapilli from Chachani contrasts with the yellowish, andesite-dacite pumice of Misti (57%–66% SiO_2). Bread-crust bombs in scoriaceous deposits interbedded with glacier and laharic deposits

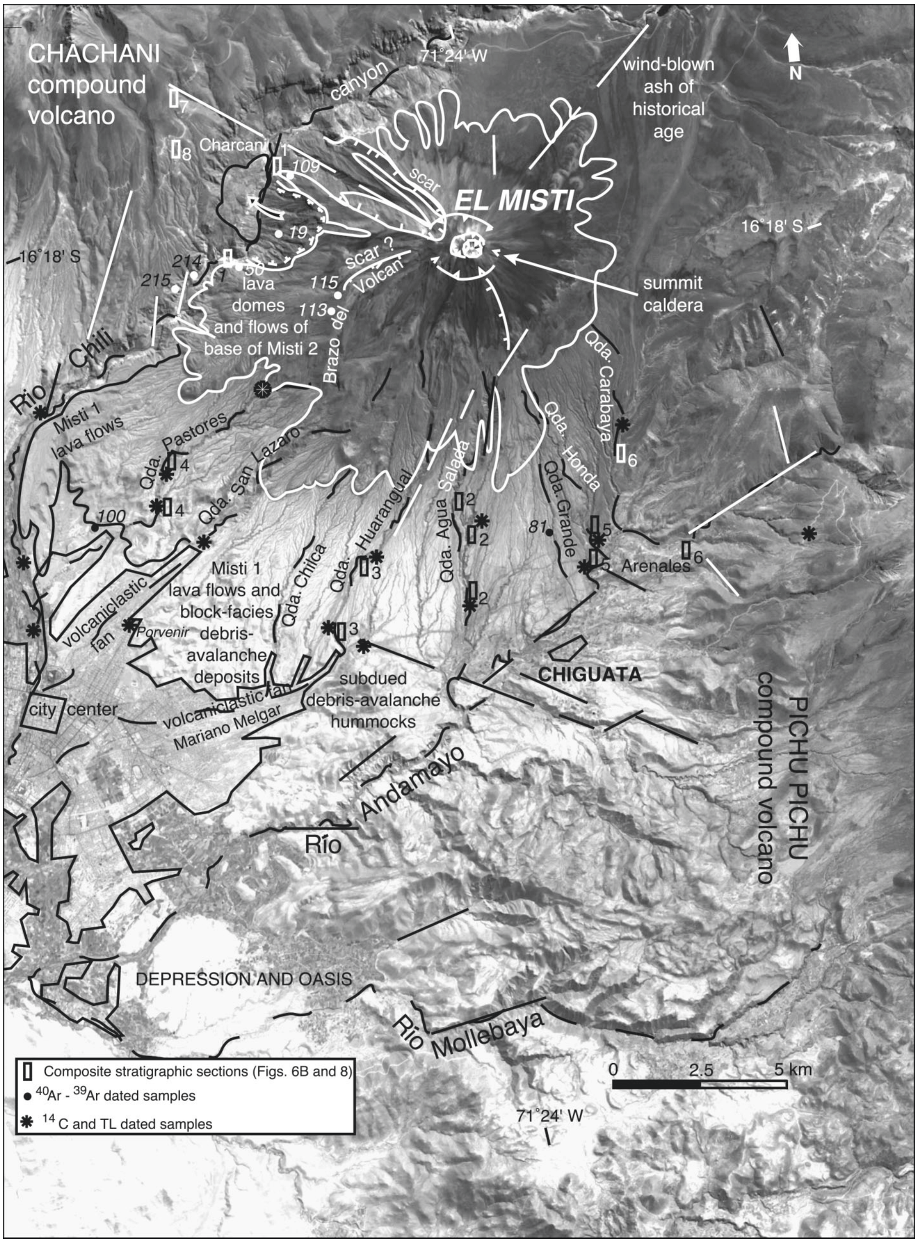

Figure 3. SPOT satellite scene (1991) showing El Misti volcano, the city of Arequipa, the main drainage channels, and important geologic features of the volcano. Qda—Quebrada (= ravine).

above 3600 masl suggest hydromagmatic interactions possibly during the *firs* Last Glacial Maximum (≥43 000 yr B.P. according to Seltzer, 1990). (Note that in the Peruvian Andes, the *second* Last Glacial Maximum occurred between 24 000 and 12 000 yr B.P..)

Stratigraphic sections in quebradas on the south flan of Misti show streamflo and lahar deposits 10–20 m thick intercalated between groups 2–2 and 2–3. The volcaniclastic deposits unconformably overlie group 2–2 and/or the greenish deposits of Chachani. The erosion interval may reveal a decrease in eruptive activity between groups 2–2 and 2–3.

Group 2–3, ca. 50–40 ka. Misti 2 (Figs. 3–5) was probably truncated above 4400 m by an incremental caldera collapse or by a cluster of large craters between ca. 50 000 and 40 000 yr B.P. (Table 2). The interpretation of an incremental caldera collapse is based on three lines of evidence.

1. A break in slope about 4400 masl separates the Misti cones 2 and 3 to the south, east, and northeast, where Misti 3 lava flow rest unconformably on block-lava flow and domes of Misti 2 (Figs. 2A, 3, and 4).

2. Nonwelded ignimbrites of 3–5 km^3 bulk volume (NI2 in Fig. 4; area is >100 km^2 and the ignimbrite deposits are 30–40 m thick on average) are found on the southwest, south, and southeast flank of the volcano; these form groups 2–3A and 2–3B (Fig. 2A; Fig. 6, col. A). Pumiceous and lithic pyroclastic-flo deposits topped by dacite pumice cobbles (Quebrada Huarangal, Fig. 7A) reflec large-scale pyroclastic eruptions that may have led to the formation of an incremental caldera collapse. On the basis of ^{14}C dating, the 2–3A subgroup erupted at ca. 50 000–43 000 yr B.P. and the 2–3B subgroup erupted at ca. 40 000 yr; thus, two distinct explosive episodes may have emplaced the ignimbrites (Fig. 6, col. A; Fig. 8, cols. 1–4; Table 2).

3. A structural boundary 4400 ± 300 masl is inferred from geoelectric self-potential (SP) measurements. The method consists of measuring differences in electric potentials between two electrodes. Differences in electric potentials are related to flui circulation within active volcanoes. The SP method aims to outline the extent of hydrothermal systems to reveal structural boundaries such as a buried caldera (e.g., Zablocki, 1976; Jackson and Kauahikaua, 1987). The SP map of Misti superimposed on a digital elevation model (DEM; Fig. 9) shows an SP minimum (with a low of 4.2 V [volts] in magnitude) that connects in a roughly rectangular shape measuring 6 × 5 km. This SP minimum divides the stratocone into (1) the lower half with negative correlation between SP values and elevation and (2) the upper half with positive correlation. This pattern, common on active volcanoes, is interpreted to be the result of electrofiltratio by downward flo of vadose water on the lower flank and upward flo of hydrothermal fluid on the upper flanks Hence, the cone shows two distinct areas: hydrogeologic and hydrothermal (Fig. 10). The upper limit of the hydrogeologic zone is located at the foot of Misti 3. The SP low appears to outline a structural boundary, interpreted as rims of large craters or of an incrementally formed caldera, that prevents the hydrothermal system from growing laterally. A 100°-trending normal fault dipping 70° toward the summit parallels the presumed boundary to the north, and 10°–40°-trending faults parallel the presumed structural boundary to the west and east (Figs. 1, 4, and 9).

Two additional methods reveal a discontinuity supporting the hypothesis of a structural boundary at ~4400 masl. A morphometric analysis of the slopes and shape of the stra-

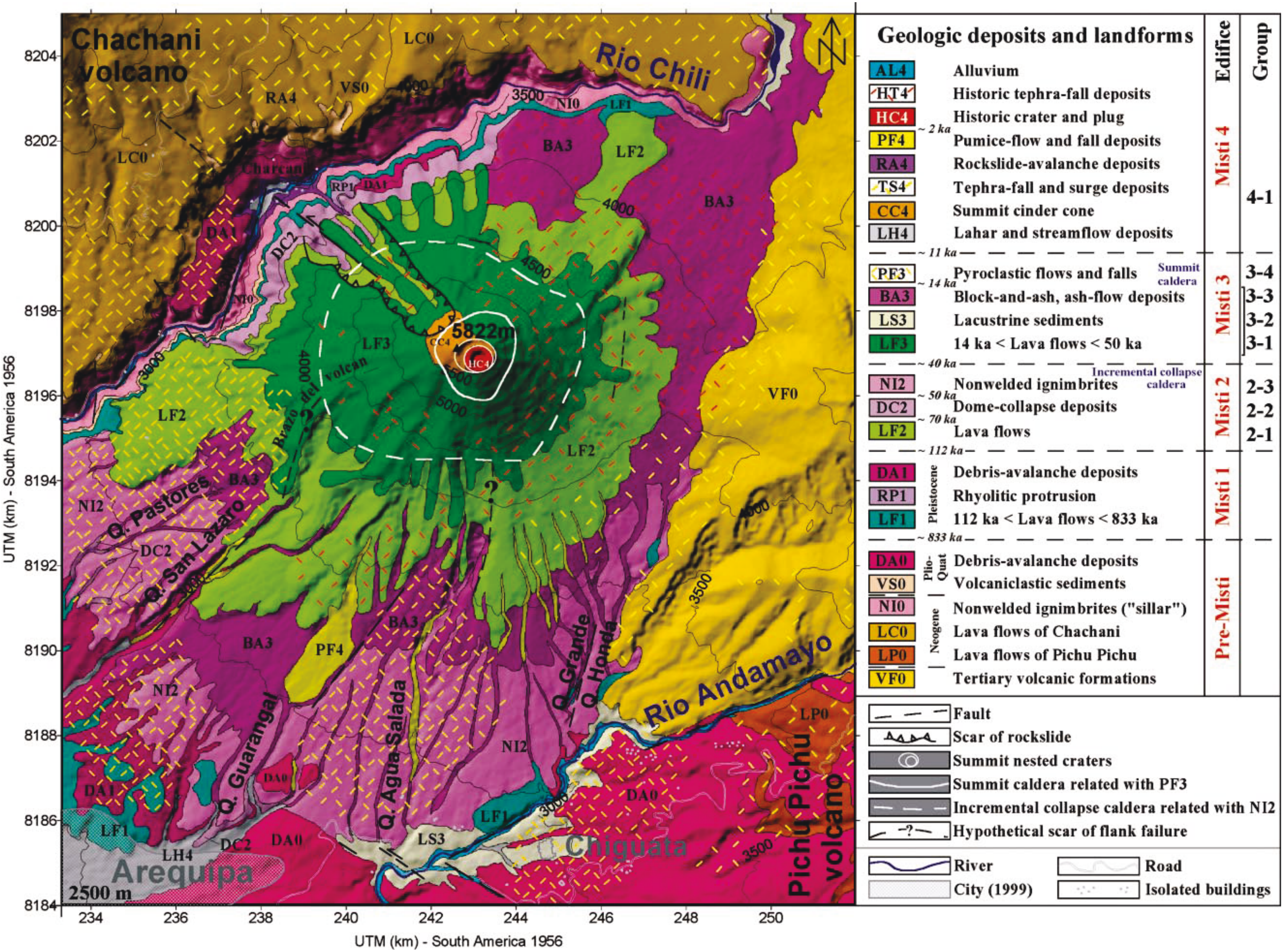

Figure 4. Geologic map superimposed on a DEM (digital elevation model). Only the most voluminous stratigraphic groups have been mapped, although the architecture of the pyroclastic ring plain comprises several piled groups. Tephra-fall deposits of group 4–1 cover the mapped area. Qda—Quebrada(= ravine).

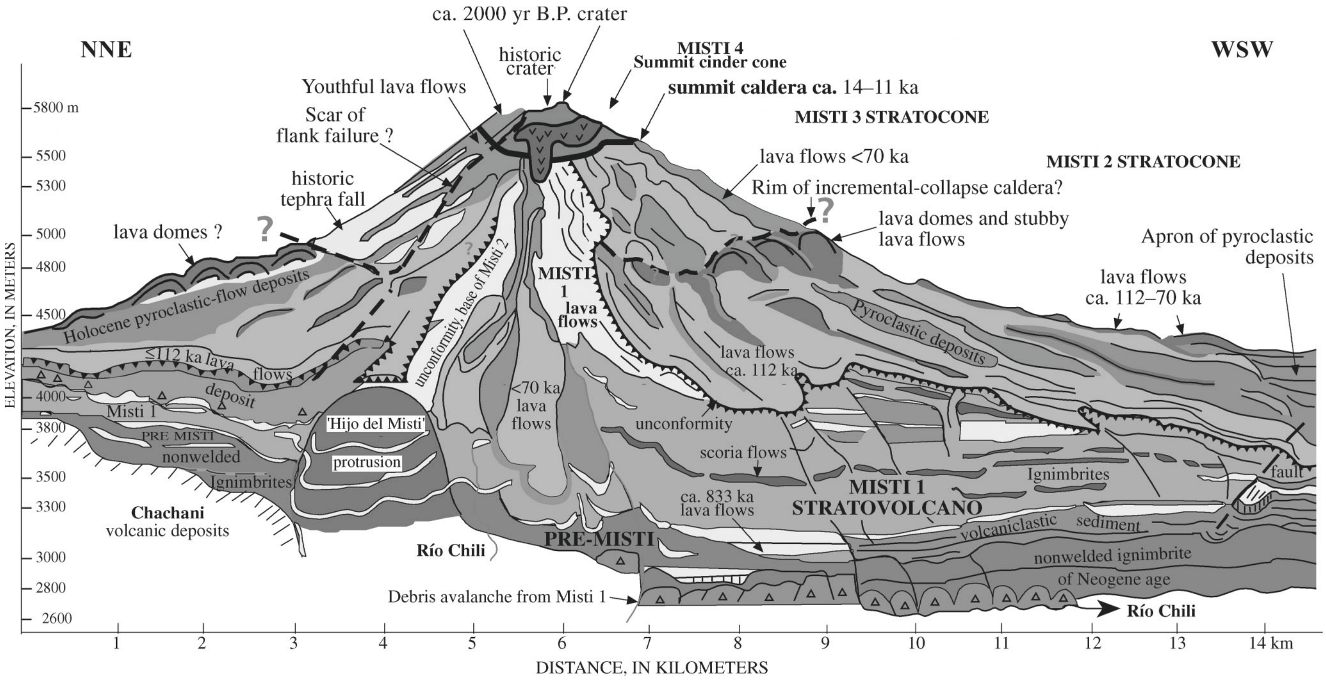

Figure 5. Schematic geologic cross section of the north to southwest flank of El Misti volcano (east bank of the Río Chili canyon), showing the pre-Misti bedrock, the Misti 1 stratovolcano, the Misti 2 and 3 stratocones, and the Misti 4 summit cone. The presumed incremental caldera on Misti 2 and the summit caldera on Misti 3 are outlined.

tocone based on a DEM shows a major discontinuity at 4400 masl (García-Zuñiga and Parrot, 1998). A controlled-source audio-magnetotelluric method, carried out by K. Pistre (2000, personal commun.), aimed at obtaining resistivity values as a function of depth on El Misti. A large (100 m) zone of low resistivity, in the range of 10–25 Ω·m, coincides with the self-potential transition zone between the hydrogeologic and hydrothermal areas. Mineralization and argillization due to circulation of hydrothermal fluid along the structural boundary may explain why resistivity is very low in the transition zone.

Misti 3 Stratocone

Misti 3 was built up of lava flow and domes (LF3 in Fig. 4; Fig. 6, col. A; Table 2) between the elevations of ~4400 and 5600 masl. The eruptions were probably after 50 000 but before 14 000 yr B.P., a period that overlapped the formation of groups 3–1 to 3–3.

Group 3–1, ca. 36–31 ka. To the southwest and southeast, a thick pile of dacitic ash-flo deposits and tephra-fall deposits forms group 3–1 (BA3 in Fig. 4; Figs. 7B and 8, cols. 2 and 5). Charcoal in soil at the base of group 3–1 yielded ^{14}C ages of ca. 34 000–33 000 yr B.P. (Table 2) in and beneath the ignimbrites (Quebrada Honda-Grande, Fig. 8, cols. 2 and 5). Radiocarbon dates on ash-flo deposits in group 3–2 indicate that the top of the dacitic group is older than ca. 31 200 yr B.P. (Fig. 8, col. 5). These pyroclastic deposits at least 1.5 km^3 in volume reflec a large explosive episode that may have enlarged the craters or the probable incremental-collapse caldera on Misti 2. On the south-southeast flan of El Misti, yellowish, dacitic pumice-flo , and tephra-fall deposits that overlie one dacitic lava flo are interbedded with groups 2–3 and 3–1. A pumice cobble from one flo deposit yielded a TL age of 36.1 ± 6.8 ka (Fig. 8, col. 3; Table 1).

Group 3–2, ca. ≤30–25 ka. The voluminous group 3–2, containing 30–50-m-thick dacitic block-and-ash-flo and lithic pyroclastic-flo deposits, mantles an extensive area on the south-southwest flan (BA3 in Fig. 4). The pyroxene- and amphibole-bearing andesite succession includes pumice-fall layers 20–40 cm thick as far as 12 km from the summit (Fig. 6, col. A; Fig. 8, cols. 1–3). Block-and-ash-flo deposits record episodes of growth and destruction of domes that have built up Misti 3 between ≤30 000 and ca. 25 000 yr B.P. (Fig. 6, col. A; Table 2). Yellow-greenish pyroclastic-flo and tephra-fall deposits 10–15 m thick are interbedded with groups 3–2 and 3–3 on the southeast flan of El Misti (Fig. 8, col. 5).

Group 3–3, ca. ≤25–20 ka. An andesitic succession encompasses as much as fiv block-and-ash-flo units 5 to 20 m thick on the south flan (BA3 in Fig. 4; Fig. 8, col. 5). These units suggest growth and destruction of domes of Misti 3 between ca. ≤25 000 and ca. 20 000 yr B.P. (Table 2). The block-and-ash-flo deposits include pumice-fall deposits whose grain size and thickness increase toward the volcano's summit, thus showing Misti as the source. The youngest of the pumice-fall layers erupted at ca. 21 ka (Fig. 8, col. 3); one pumice cobble from the second pumice-fall layer was dated at ca. 20.3 ka (TL, Table 1). The most voluminous (≤0.5 km^3) Plinian pumice-fall deposit of El Misti is 1 to 3 m thick at distances of 9–12 km west and southeast of the vent (Figs. 7C and 8, col. 6).

In the upper radial valleys, toward the top of group 3–3, debris-flo and stream-flo deposits are interbedded with block-and-ash-flo and scoria-flo deposits including phreatomagmatic bombs. In U-shaped valleys probably carved by glaciers on the southeast flan of Chachani above 3600 masl, stratifie layers of ash with subrounded pumice were emplaced in water and probably formed terraces on the edge of former glacier tongues (Fig. 7C). Tephra deposits were likely reworked by meltwater from ice field that capped the Misti and Chachani summits during the second Last Glacial Maximum (between 24 000 and 12 000 yr B.P.; Seltzer, 1990).

Summit Caldera on Misti 3, Group 3–4, ca. 14–11 ka. Misti 3 was in turn truncated

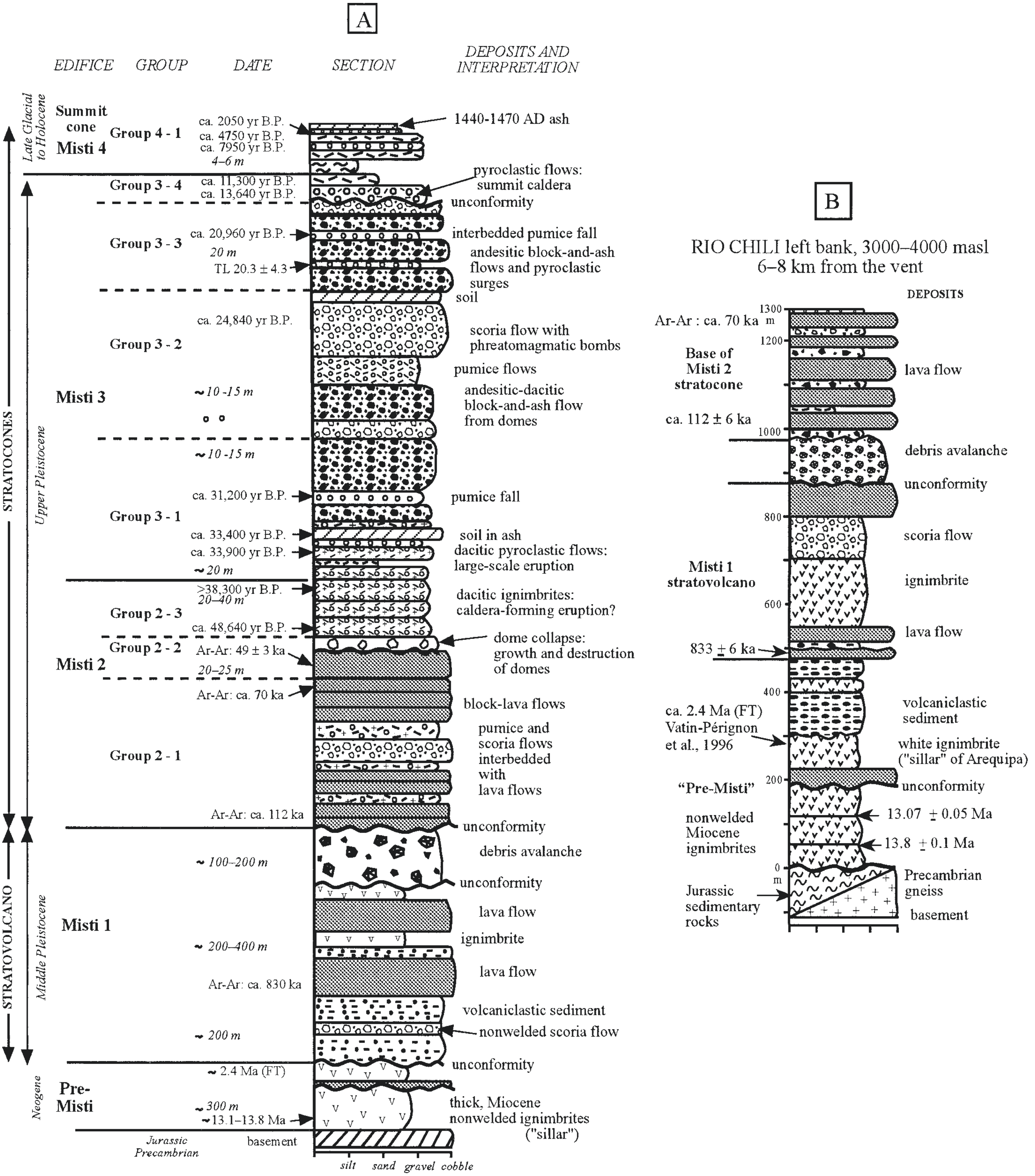

Figure 6. (A) Composite stratigraphic section of pre-Misti, Misti 1, and groups of Misti 2–4 cones based on measured columns (located in Fig. 8). (B) Composite stratigraphic section on the left bank of the Río Chili canyon showing pre-Misti and Misti 1–2 deposits.

TABLE 1. SELECTED ^{40}Ar-^{39}Ar AND TL AGES AT MISTI VOLCANO

Samples number		Location (in Fig. 3)	Elevation (m)	Edific	Group (ka)	Age (ka)
Mi 81	Whole rock	Qda. Honda	3250	Misti 3?	Group 3–1?	49 ± 3
Mi 115	Whole rock	Brazo del Misti	4400	Misti 2	Group 2–2	70 ± 3
Mi 113	Whole rock	Brazo del Misti	4000	Misti 2	Group 2–1	98 ± 3
Mi 109	Whole rock	Rio Chili, Charcani V	3600	Misti 2	Group 2–2	105 ± 2
Mi 50	Whole rock	Pacheco torres Rio Chili	3350	Base of Misti 2	Group 2–2	112 ± 6
Mi 100	Whole rock	Rio Chili downstream Charcani I	2800	Base of Misti 1		833 ± 6
Mi 214	On biotite	Rio Chili canyon, Charcani III	2800	Pre-Misti ignimbrite		13.12 ± 0.05 Ma
Mi 215	On biotite	Rio Chili canyon, Charcani III	2880	Pre-Misti ignimbrite		13.8 ± 0.1 Ma
Thermoluminescence on plagioclase in pumice						
TL Mi 200b		Huarangero dirt road	2850		Group 3–3	20.3 ± 4.3
TL Mi 200		Qda. Huarangal	2800		Group 3–1	36.1 ± 6.8

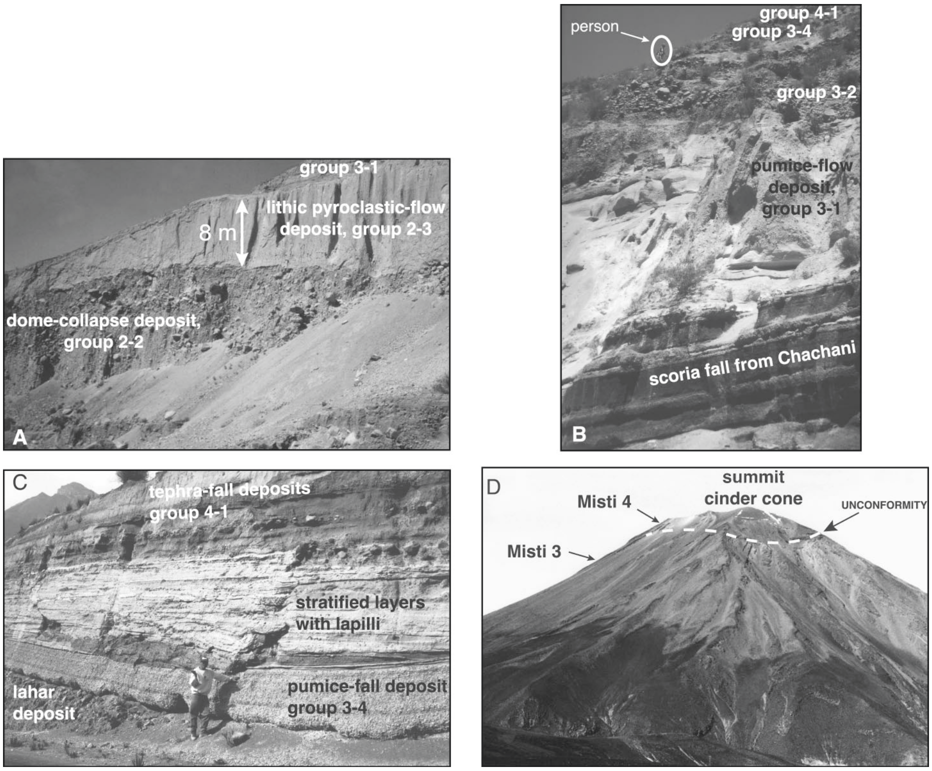

Figure 7. (A) Quebrada Huarangal section 11 km from the vent showing pyroclastic deposits of groups 2–2 and 2–3. (B) Section 20 m thick in Quebrada Pastores 9 km from the vent showing andesitic scoriaceous fall deposits of Chachani, overlain by pyroclastic deposits of groups 3–1, 3–2, 3–4, and 4–1. (C) Section 8 km west of the summit (road to Charcani, 3600 masl) showing a 1-m-thick pumice-fall deposit of group 3–4 above lahar deposits and overlain by stratifie layers of reworked ash and tephra-fall deposits of group 4–1. (D) Northwest flan of El Misti with unconformity surrounding the summit caldera at ~5400 masl.

by formation of a summit caldera 2 km across above the elevation of 5400 m (Figs. 3–5). Evidence for a summit caldera is threefold:

1. Cliffs of welded scoria-flo deposits on the west-northwest summit slope (at 5400 masl) and lava flow unconformably overlie steep lava flow of Misti 3 dipping to the west (Fig. 7D).

2. Pyroclastic-flo deposits of ~1 km³ bulk volume (PF3 in Fig. 4; area ~50 km² × 20 m thickness) with interbedded pumice-fall and pyroclastic-surge beds (≤0.5 km³) form group 3–4 (Fig. 4). A voluminous, 1-m-thick pumice-fall deposit, 9 km west of the vent (Fig. 7C), is stratigraphically beneath one of the thick scoria-flo deposits dated at ca. 13 700 yr B.P. (Fig. 8, cols. 2 and 5). At the base of the interbedded pumice-fall deposits, group 3–4 also contains 10–20-cm-thick cross-bedded layers of gray lithic ash with oxidized fragments that form pinch-and-swell and dune-like features (Fig. 8, cols. 2, 4, and 6). These layers are interpreted as pyroclastic surges that traveled as far as 12 km south and southwest of the vent. The radiocarbon dates indicate that the deposits were emplaced in two explosive eruptions between ca. 13 700 and 11 300 yr B.P. (Fig. 6, col. A; Fig. 8, cols. 2 and 5; Table 2). These dacitic deposits may reflec caldera-forming eruptions.

3. An elliptical structural boundary (2 × 1.5 km) is inferred from a secondary self-potential minimum ~5400 masl (Figs. 9 and 10). A morphometric analysis of the stratocone also reveals a structural discontinuity at ~5400 masl (García-Zuñiga and Parrot, 1998).

Misti 4 Summit Cone, Group 4–1, <11 ka

The crescent-like summit is a cinder cone (CC4 in Fig. 4) designated Misti 4, which formed above the summit caldera of Misti 3. Welded scoria-flo or fall deposits buried the west part of the caldera, but two nested craters were opened in the central and eastern areas of the caldera (Fig. 11A). The 950-m-wide crater, breached to the south, may have been formed during a ca. 2300–2050 yr B.P. explosive episode. The nested scoria-rimmed crater, 550 m across and 200 m deep, cut domes in historic time. It is blocked by an andesite plug, where fumarolic activity persists (Fig. 11B).

A 5–6-m-thick pile of tephra-fall deposits indicates that Misti 4 erupted tephra at least 10 times since 11 000 yr B.P. (TS4 in Fig. 4; Fig. 8, cols. 2 and 5). The tephra-fall beds are intercalated in scoriaceous ash-flo deposits on the southwest to southeast flanks Thin, cross-bedded, dune-like ash layers, interpreted as pyroclastic surges similar to those of group 3–4, traveled 8 km southeast toward Chiguata (≥6400 yr B.P.) and 13 km southwest toward the Río Chili valley (ca. 5200 yr B.P.; Figs. 4 and 8, col. 4). Two pyroclastic-surge deposits were emplaced just before ca. 11 300 yr B.P. and as recently as ca. 4750 yr B.P. in what is

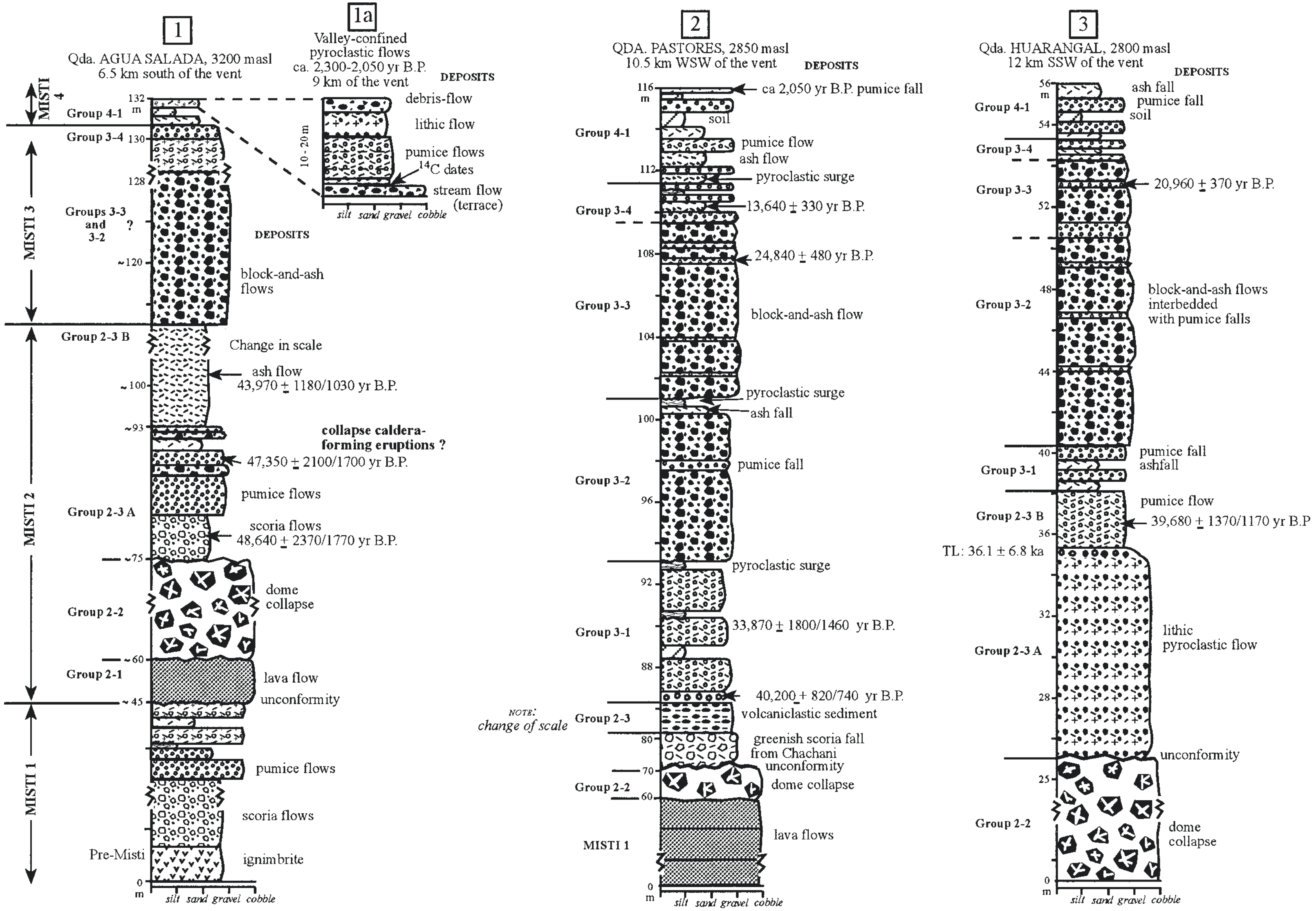

Figure 8. Eight composite stratigraphic sections of El Misti deposits (located in Fig. 3). ^{40}Ar-^{39}Ar dates, ^{14}C dates, and TL measurements in Table 1 and 2 and Data Repository (see text footnote 1).

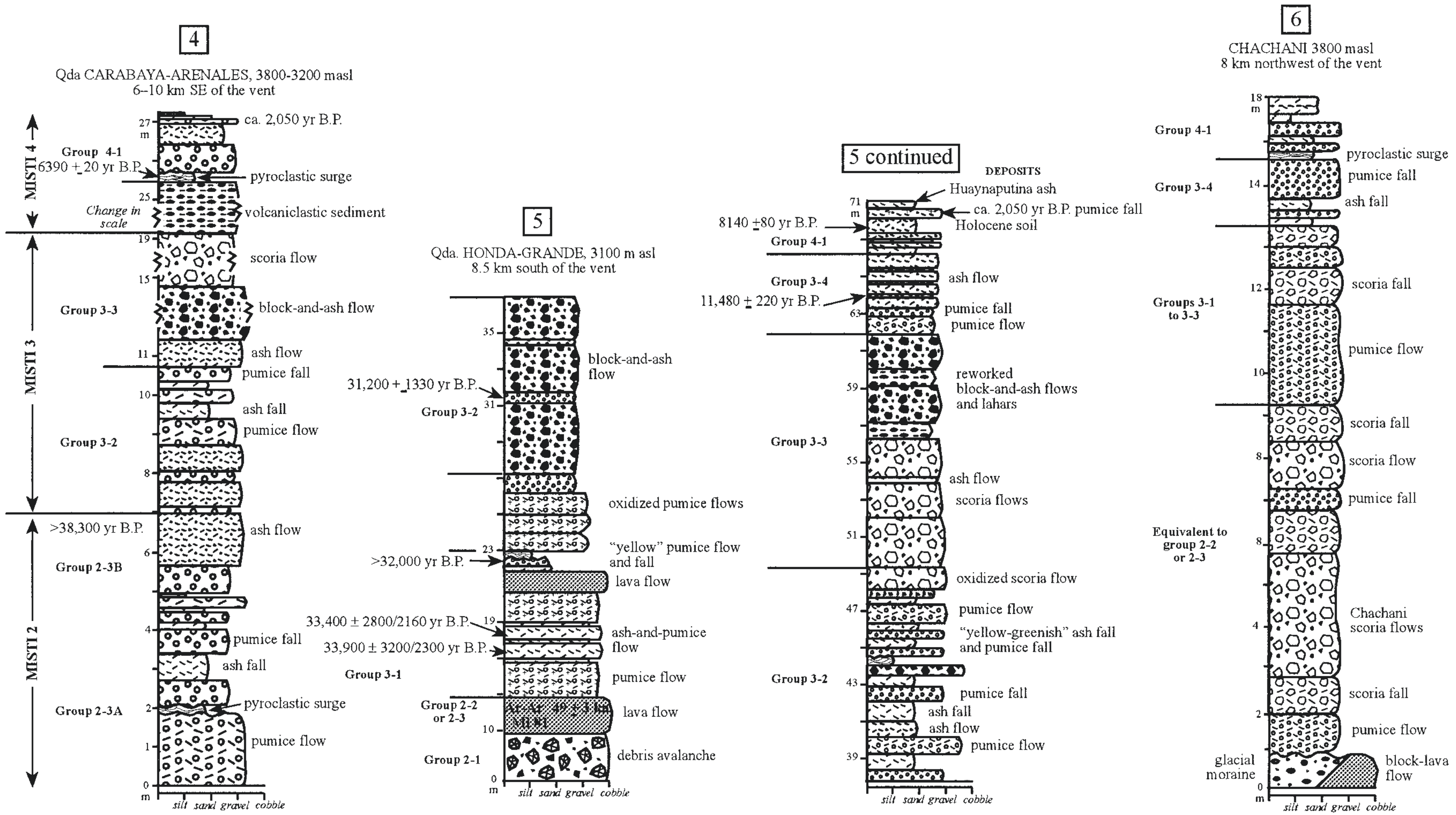

Figure 8. (*Continued.*)

TABLE 2. LIST OF 14 C DATES

Sample number	Location (Figs. 3, 5, and 10)	Material	Deposit	Group	^{14}C age (yr B.P.)	Calibrated age (1 σ)
GrN-23966	Academia Yanahuara, Río Chili, Arequipa	Charcoal	Lahar	Middle terrace	520 ± 25	1407–1428 cal A.D.
GrN-23965	Río Chili, Chocita	Charcoal	Silt	Low terrace	340 ± 40	1488–1633 cal A.D.
GrN-23888	Qda. Huarangal entrada Mariano Melgar	Charcoal	Streamflo	Volcaniclastic fan	13650 ± 300/290	
GrN-22163	Qda. Huarangal arriba	Organic matter	Tephra fall	Group 4–1	620 ± 50	1304–1398 cal A.D.
GrN-23985	Qda. Grande arriba, tributary	Charcoal	Soil in ash	Group 4–1	1290 ± 100	655–865 cal A.D.
Lv-2111	Qda. San Lazaro	Charcoal	Pumice fall	Group 4–1	1920 ± 200	160 cal B.C.– 340 cal A.D.
GrN-23149	Qda. Honda	Charcoal	Pumice fall	Group 4–1	2060 ± 40	106 cal B.C.– 2 cal A.D.
GrN-22162	Qda. Honda	Charcoal	Pumice fall	Group 4–1	2090 ± 40	160–46 cal B.C.
GrA-4398	Qda. Agua Salada	Charcoal	Pumice flo	Group 4–1	2300 ± 60	402–208 cal B.C.
GrN-23964	Rio Chili valley, Garita B	Charcoal	Ash fall	Group 4–1	3800 ± 50	1991–2465 cal B.C.
GrA-11253	El Porvenir,Alto Misti, Arequipa	Charcoal	Surge	Group 4–1	4750 ± 40	3635–3385 cal B.C.
GrN-23963	Rio Chili valley Garita A	Charcoal	Surge	Group 4–1	5200 ± 80	3822–4220 cal B.C.
GrA-13242	Qda. Carabaya	Organic matter	Ash flo beneath surge	Group 4–1	6390 ± 50	5465–5317 cal B.C.
GrA-11459	Qda. Honda	Charcoal	Ash flo	Group 4–1	8140 ± 80	7315–7057 cal B.C.
GrN-23961	El Porvenir,Alto Misti, Arequipa	Charred wood	Pumice flo above surge	Group 3–4	11280 ± 70	11389–11205 cal B.C.
GrN-24114	Qda. Honda abajo Tributary	Charcoal	Ash flo	Group 3–4	11340 ± 240	11805–11075 cal B.C.
GrN-24038	Qda. Honda	Charcoal	Tephra fall	Group 3–4	11480 ± 220	11845–11225 cal B.C.
GrN-23658	Qda. Pastores arriba	Charcoal	Scoria flo	Group 3–4	13640 ± 330	
GrN-23889	Qda. Huarangal Huarangero	Charcoal	Pumice fall	Group 3–3	20960 ± 380/360	
GrN-23247	Qda. Pastores	Charred wood	Block-and-ash flo	Group 3–3	24840 ± 480	
GrN-23246	Qda. Honda-Grande confluenc	Charcoal	Block-and-ash flo	Group 3–1	31200 ± 1330	
GrN-24037	Qda. Honda-Grande confluenc	Charcoal	Ash flo	Group 3–1	>32,000	
GrN-23659	Qda. Pastores Tributary	Charcoal	Ash flow	Group 3–1	33400 ± 2800/2160	
GrN-21574	Qda. Pastores	Organic matter in soil		Group 3–1	33870 ± 1800/1460	
GrN-24325	Qda. Honda- Grande abajo	Organic matter	Ash flo	Group 3–1	33900 ± 3200/2300	
GrN-24113	Arenales	Charcoal	Ash flo	Group 2–3B	>38300	
GrN-23887	Qda. Huarangal arriba	Charcoal	Block-and-ash flo	Group 2–3B	39680 ± 1370/1170	
GrN-23884	Río Chili, garita	Charcoal	Pumice flo	Group 2–3B	40200 ± 820/740	
GrN-23962	Qda. Agua Salada abajo	Charcoal	Ash flo	Group 2–3A	43970 ± 1180/1030	
GrN-22884	Qda. Agua Salada Abajo	Charcoal	Pumice flo	Group 2–3A	47350 ± 2100/1700	
GrN-23890	Qda. Agua Salada arriba, tributary	Charcoal	Scoria flo	Group 2–3A	48640 ± 2270/1770	

Note: (GrN numbers—conventional dates; GrA numbers—AMS dates; J. van der Plicht, Center for Isotope Research, Groningen) obtained on pyroclastic and lahar deposits, and soils of groups 2–3 to 4–1.

now the Porvenir suburb of Arequipa, 13 km from the vent. Soils in the tephra pile are poorly developed, even in the wettest altitudinal vegetation belt (3200–3800 masl). Their poor development suggests that explosive activity ceased for only short periods. Wavy ash beds and truncated lenses with small subrounded pumice indicate that runoff and/or eolian processes removed ash deposits of Holocene age. Similar wavy and truncated ash beds toward the top of sections are underlain by ≥6400 yr B.P. primary flo and fall deposits and overlain by a dark soil mixed with a ca. 3800 yr B.P. ash-fall layer in the Río Chili valley (Fig. 8, col. 4; Table 2). Wind action may have been enhanced during the driest Holocene period between ca. 8200 and ca. 3600 yr B.P., evidenced in the area of Lake Titicaca, 150 km east of Misti (Seltzer et al., 1998).

The dry middle Holocene interval contrasts with the late glacial and early Holocene periods when debris-flo and stream-flo deposits formed the two volcaniclastic fans upon which the city of Arequipa has been built (Fig. 3). Runoff and flas flood triggered by rainstorms, common in January–February, cut into the late glacial–early Holocene volcaniclastic deposits dated between ca. 13 700 and 8000 yr B.P. that fille the stream channels (LH4 in Fig. 4).

EXPLOSIVE ACTIVITY OVER THE PAST 2300 YR

The Most Recent Sub-Plinian Episode, ca. 2300–2050 yr B.P.

Pumice-flo and fall deposits of the last major explosive episode of El Misti are portrayed in Figure 12. We determined two calibrated ca. 2300 yr B.P. ^{14}C ages at the base of pumice-flo deposits in Quebrada Agua Salada and three ca. 2050 yr B.P. ages at the base of pumice-fall deposits in Quebrada San Lazaro (Thouret et al., 1995; Table 2). Whether the error range in ^{14}C ages encompasses one or a few discrete eruptions is not yet established.

A pumice-fall deposit dispersed ≥25 km southwest toward Arequipa includes three layers, totaling 30 cm thick, 13 km southwest of the vent. Accidental lithic and accessory oxidized fragments of the upper coarse sand layer are more abundant than in the lower layer, which is rich in coarse pumice lapilli. The banded pumice includes layers of rhyolite (71% SiO_2) and andesite (63% SiO_2) composition. A thin, interbedded, middle layer of coarse sand, and nonvesicular lithic fragments indicates that the eruption column dwindled just before the second layer was emplaced, probably owing to erosion of the conduit. From the isopachs of the pumice-fall deposit, bulk volume amounts to ~0.1 km^3 (Fig. 12). From the isopleths in Figure 12, the height of

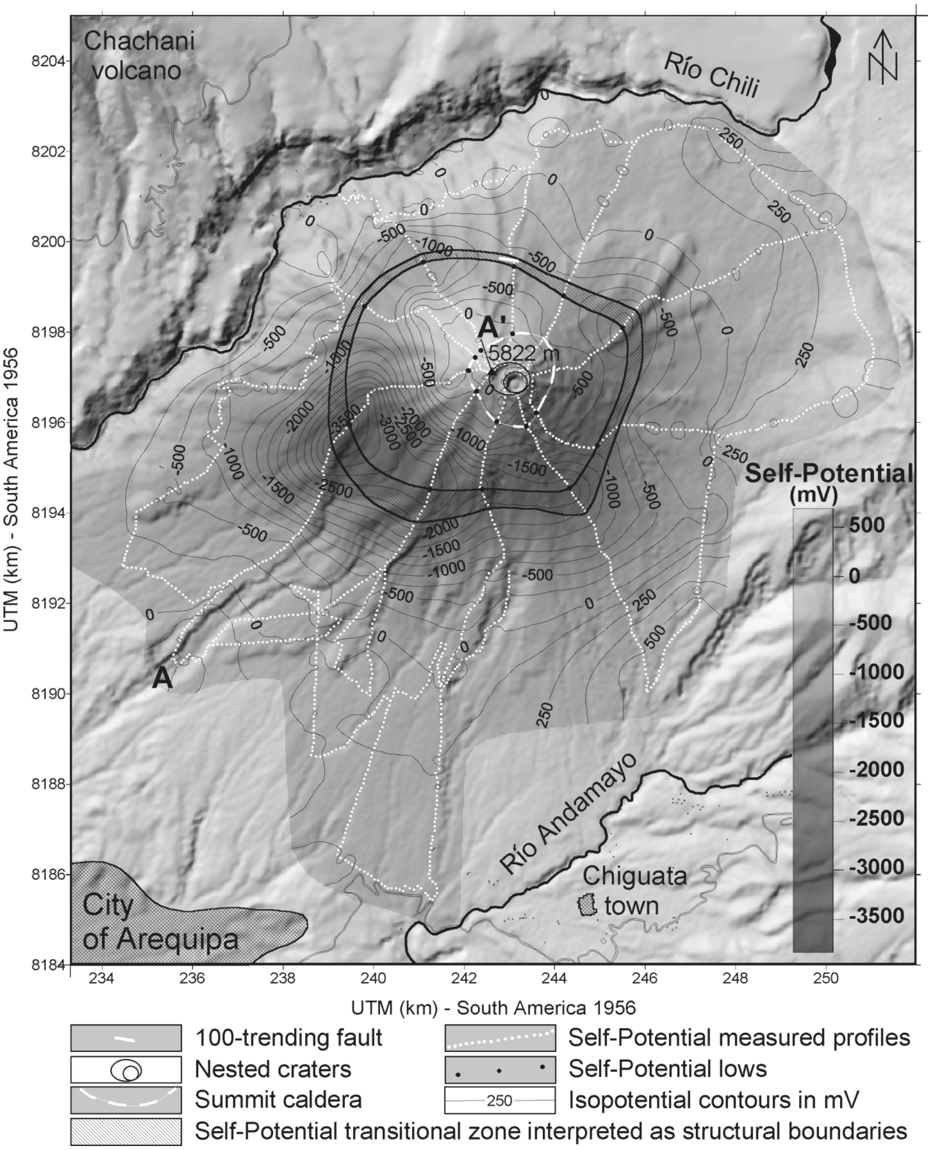

Figure 9. Self-potential map superimposed on a DEM of El Misti volcano. The A–A′ profil is shown in Figure 10.

the sub-Plinian column was in the range of 10–13 km above the vent.

Nonwelded pumice-rich flow with a volume of ≤0.7 km³ were channeled in all radial valleys as far as the present suburbs of Arequipa and 2 km upstream from the town of Chiguata (PF4 in Fig. 4; Fig. 8, col. 1; Fig. 11C). No fall deposit underlies the voluminous flo deposits in the south catchments (Quebrada Agua Salada, Fig. 8, col. 5). However, several open-work pumice lenses interbedded with 4 to 6 flo units suggest that the eruption column collapsed on the south flan during the tephra fall. At ~3400 masl, the 30-m-thick pyroclastic-flo deposits are pumice-rich, whereas the uppermost unit is rich in coarse, accessory, oxidized lithic cobbles. Abundant lithic cobbles in the uppermost flo unit suggest that the large crater reamed out the summit cone and/or breached during the eruption. Alternatively, a lithic-rich flo was decoupled from the pumice-rich flow during transport because clasts are gradually segregated from the lower pumice-flo deposits up toward the cobble-rich deposit.

Lahar deposits overlie the ca. 2050 yr B.P. pyroclastic-flo deposits, but pinch-and-swell lenses of pumice-flo deposits are interbedded with pumice-rich lahar deposits 2–4 km from the front of the pumice-flo deposits (Quebrada San Lazaro, 13 km from the vent). These sedimentary features suggest that pumice-rich flow were rapidly transformed into lahars immediately after the eruption. The ca. 2300–2050 yr B.P. explosive episode may have also destabilized the steep, fractured west-northwest flank as suggested by rock-slide avalanche and lahar deposits rich in oxidized and scoriaceous blocks that form terraces of similar age in the upper Río Chili canyon (RA4 in Fig. 4).

Moderate Explosive Activity in Historic Time

Eruptions were not recorded until the founding of Arequipa in 1540 by the Spanish. However, youthful pyroclastic deposits, widespread on the north, south, and southeast flank of the volcano toward the town of Chiguata (HT4 in Fig. 4; Fig. 8, cols. 1 and 4), record a few historical eruptions younger than 2050 yr B.P.

Youthful ash-rich flo deposits form two prominent fronts at ~3800 and 3400 masl on the southeast flan of Misti. A gray ash-rich flo deposit 4 m thick shows dune-like landforms as far as 9 km south of the vent near Quebrada Honda-Grande (3200 masl). Charcoal in soil beneath the ash-flo deposit in this area yielded a ^{14}C age of ca. 1300 yr B.P. (Table 2). However, the small volume of tephra-fall deposits indicates that explosive activity was mild. An ash layer interbedded in a block-and-ash-flo deposit on the south flan (Quebrada Huarangal, 3800 masl) is dated at ca. 620 yr B.P. (Table 2).

A scoriaceous ash-fall layer of andesitic composition is at least as thick as 10 cm on the cone slopes and 2–4 cm in the Arequipa area (Fig. 12). A black ash layer beneath the A.D. 1600 Huaynaputina ash (Thouret et al., 1999b) records the A.D. 1440–1470 eruptive event, as referred to in anecdotal narrations (Chávez Chávez, 1992). Complaints of the distressed population were such that the Inca emperor, Pachacútec, sent his wife to help the people of Chiguata. A fine-san ash is 1 cm thick 30 km west and 20 km north of the volcano and 0.5 cm thick 25 km east in Laguna (Lake) Salinas (Fig. 1; Juvigné et al., 1997). The dispersal lobe (Fig. 12) and the thickest scoria fall on opposite crater rims (Fig. 11A) indicate that discrete Vulcanian eruptions occurred when winds were blowing east-northeast and west-southwest. Both the lack of ballistic scoria or lithic blocks and the sand size of the ash-fall deposit outside the crater area suggest that the eruptive columns were low. The irregular thickness of the thin ash layers and the amount of small xenolithic fragments from the underlying soil and overlying Huaynaputina ash indicate that runoff and wind

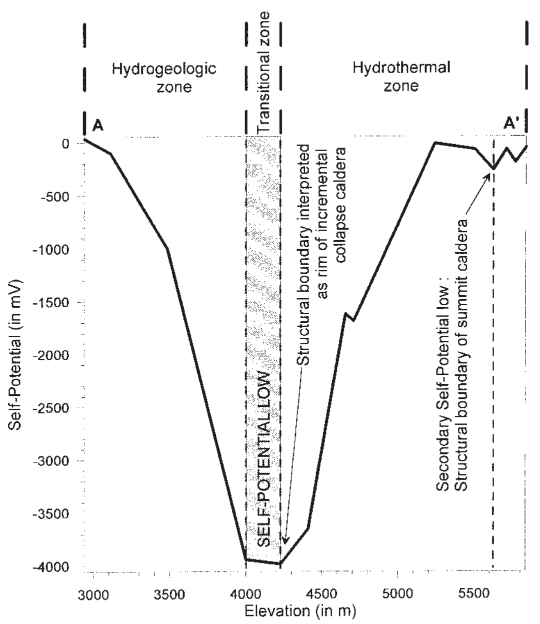

Figure 10. Composite cross section of the measured self-potential profile showing self-potential versus elevation. The boundaries of the hydrogeologic and hydrothermal zones and profil A–A′ are shown in the accompanying map (Fig. 9).

have mixed the black ash with surficia deposits between small-scale Vulcanian events.

Historic eruptions of Misti may be indirectly recorded as two matrix-supported lahar deposits mantling the middle and lower terraces of the Río Chili in the city of Arequipa. Silt- and sand-sized deposits 1–3 m thick that include ash and oxidized pyroclastic fragments have been dated at ca. 520 yr B.P. (A.D. 1407–1428 [calibrated ^{14}C date]) and ca. 340 yr B.P. (A.D. 1488–1633 [calibrated ^{14}C date], Table 2). Although the link with the events of A.D. 1400–1600 cannot be demonstrated, the A.D. 1440–1470 eruption may have triggered lahars, as ash has been incorporated in the matrix-supported debris-flo deposits with a volume of $1.5–3 \times 10^6$ m^3.

After the Spanish conquest, the record of volcanic activity at Misti mentions several questionable events: 1542?, 1599?, August 1826?, August 1830 and 1831?, September 1869, and March 1870? (Hantke and Parodi, 1966; Simkin and Siebert, 1994). Available narrations (Zamácola y Jaureguí, 1804; Barriga, 1951; Chávez Chávez, 1992) suggest that these events were episodes of increased fumarolic activity. However, three seismic and possibly phreatic events occurred on 2 May 1677, 9 July 1784, and 28 July and 10 October 1787 (VEI 2? [VEI—volcanic explosivity index], Simkin and Siebert, 1994). Since 1787, persistent high-temperature fumaroles have been observed on the plug and on the summit's southeast flank Fumaroles high above the crater rim were seen from Arequipa in 1948–1949 and in 1984–1985; the maximum fumarole temperature of the plug was 220 °C, measured in December 1997.

DISCUSSION

Stratigraphy and preliminary petrologic data support the following discussion on the nature and evolution of lavas and tephras and on the volume versus time relationships for the Misti cones.

Geochemistry

El Misti's magmas have been geochemically homogeneous, but the products of Misti 4 are distinct, as discussed subsequently. From the relatively homogeneous magmas erupted through time, four rock types prevail: two-pyroxene and amphibole andesites, amphibole dacites, amphibole and biotite dacites, and biotite-bearing rhyolites. Some andesites also bear apatite, and scarce andesites bear one pyroxene or amphibole only, but basaltic andesites are lacking. Lavas from Misti 2 and Misti 3 show no significan change in composition compared to lavas of Misti 1. Most of the calc-alkalic lavas belong to moderately high K_2O andesites (57.4%–62.1% SiO_2), dacites (63.5%–66.3% SiO_2), and a few rhyolites (71.7%–72.8% SiO_2; Fig. 13, after Legendre, 1999). Bulk-rock chemical analyses indicate that the magmas of Misti 2 to Misti 4 have evolved from silica rich to less silica rich through time. In contrast, group 2–2 consists of rhyolites, although they are not unknown in more recent groups.

The mineral suites of the lavas show a trend from group 2–1 toward group 4–1 (Data Repository, after Legendre, 1999). The plagioclase remains similar from group 2–1 to group 4–1 (except in the rhyolites of group 2–2) and shows a wide range of composition (An_{23}–An_{73}) and strong geochemical variations. Clinopyroxene remains relatively constant (En_{45}–En_{50}), but orthopyroxene (En_{65}–En_{80}) and calcic amphibole (pargasite, Fe-pargasite, and Fe-pargasitic hornblende) become more magnesian from group 2–1 toward group 4–1. In the contrasting group 4–1, orthopyroxene disappears whereas ilmenite (TiO_2 44%–50%) appears, and magnetite (Fe_2O_3 30%–40%) plots closer to the pure-magnetite pole. Geothermobarometers indicate the order of crystal formation (clinopyroxene, orthopyroxene, then amphibole and plagioclase) and relatively homogeneous equilibrium conditions for minerals of groups 2–1 to 3–2. However, lavas of group 4–1 reflec weaker $f(O_2)$ and less oxidizing conditions than those of the previous groups. On the basis of the equilibrium conditions indicated by the mineral phases, Legendre (1999) suggested a magma chamber depth in the range of 3–9 km. The comparison of data from stratigraphy and geochemistry leads to four results (Legendre, 1999):

1. Abundant andesites coincide with the emplacement of lava flow and/or moderate volumes of tephra that formed groups 2–1, 3–3, and 4–1. Abundant dacites and rhyolites coincide with large-scale explosive eruptions that emplaced groups 2–2, 2–3, 3–1, and 3–2 and may have led to an incremental caldera collapse.

2. Groups 2–1 and 2–2 may belong to a similar eruptive period with a differentiation from andesites to rhyolites. Rhyolites seem to be related to large explosive eruptions toward the end of Misti 2.

3. Andesites of groups 2–1 to 3–2 are similar in their mineral assemblages and geochemistry and may have formed through AFC (assimilation–fractional crystallization) in the lowermost crust. In contrast, rhyolites of group 2–2 and dacites of groups 2–2 and 3–1 may be the result of fractionation and contamination in the upper crust.

4. The lack of orthopyroxene and the presence of ilmenite in group 4–1 constitute a distinct mineral suite. This difference may reflec a change in physical conditions in the reservoir. Trace-element geochemistry (Jacquemin

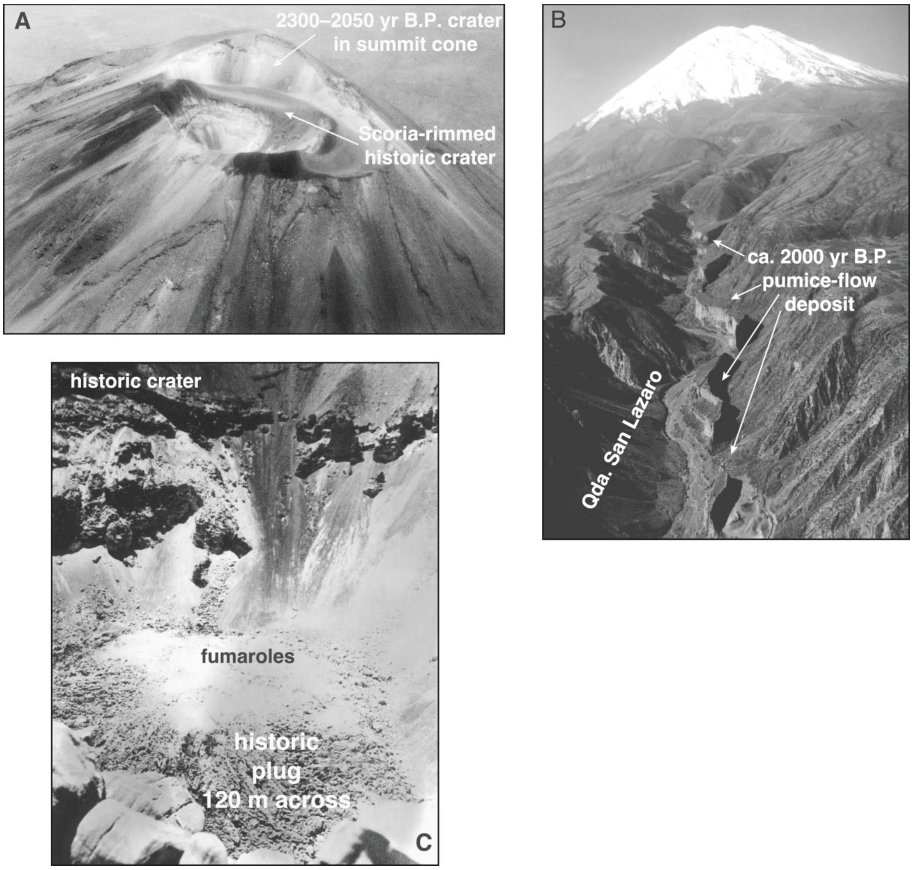

Figure 11. (A) Summit cone of Misti 4 (looking north): the historic, scoria-rimmed crater nested in a crater 950 m across, probably ca. 2300–2050 yr B.P. (B) Pumice-flo deposits 20–30 m thick, channeled >9 km in the Quebrada (Qda.) San Lazaro valley and dated at ca. 2300–2050 yr B.P. (C) Fumarolic plug in historic, scoria-rimmed crater 200 m deep.

and Joron, 1984) indicates a new andesitic magma batch.

Volume Versus Time Relationships in the Composite Misti 2–4 Stratocones

The eruption rate over the ~112-k.y.-long period of the Misti 2–4 stratocones (preserved volume of 70–83 km³) averaged 0.63 km³/k.y., but four periods of peak eruption rates (accountable for groups 2–1, 2–2, 3–2, and 3–3) may have increased the cone volumes by as much as 2.1 km³/k.y. (Fig. 14). Between emplacement of groups 2–2 and 3–1 and between emplacement of groups 3–3 and 4–1, the Misti 2 and 3 cones underwent erosion. Sustained explosive periods 2–3, 3–1, 3–3, and 4–1 have produced as much as 7–10 km³ of ignimbrites and tephra, preserved around the volcano. The amount of deposits removed from each cone and the duration of erosion intervals are not accurately known at Misti. Thus, our estimate of the growth rates of Misti 2, Misti 3, and Misti 4 cones is considered a preliminary result. However, volume versus time relationships at similar well-studied composite volcanoes (Davidson and de Silva, 2000) suggest that rates of the Misti cone-building episode are comparable to that of Mount Adams (USA) and higher than those of Tongariro (New Zealand) and Tatara–San Pedro (Chile). Volumes of deposits may be better preserved at El Misti than on these other volcanoes that are located in wetter environments with more efficien erosion by glaciers and runoff.

CONCLUSIONS

From the study of the geology and past eruptive behavior of El Misti, we have determined the following:

1. Composite El Misti comprises a stratovolcano (ca. 833 to >112 ka) designated Misti 1 and 3 stratocones (≤112 ka) designated Misti 2, Misti 3, and Misti 4. Misti 4 has been active as recently as A.D. 1440–1470, and phreatic events reportedly occurred in 1677, 1784, and 1787.

2. Seven eruptive periods have successively built up Misti 2–4 during a period of ~112 k.y. The eruption rate over that period averaged 0.63 km³/k.y.

3. Repeated episodes of growth and destruction of lava domes have triggered dome-collapse avalanches and block-and-ash flows including pyroclastic surges (e.g., group 3–2, ca. 31 000 and 25 000 yr B.P., and group 3–3, ca. 25 000 and 20 000 yr B.P.). The dome-building episodes alternated with sub-Plinian eruptions whose high columns collapsed and generated pyroclastic flow (e.g., groups 3–1, 3–3, and 4–1).

4. Nonwelded dacitic ignimbrites (groups 2–3 and 3–4) with a bulk volume of 4–6.5 km³ probably reflec large explosive eruptions that may have led to an incremental caldera collapse or formation of large craters between ca. 50 000 and 40 000 yr B.P. and again to a summit caldera between ca. 13 700 and 11 300 yr B.P.

5. Misti 4 erupted less evolved andesites with a distinct mineral suite, compared to that of Misti 2 and Misti 3. Scoria-flo and fall deposits of Misti 4 are related to the formation of the summit caldera at ca. 13 700–11 300 yr B.P., the nested craters, and the A.D. 1440–1470 event. A decrease in SiO_2 content in the products of group 4–1 indicates injection of a new andesite magma batch, but the ca. 2050 yr B.P. banded pumice of rhyolitic and andesitic composition suggests a process of magma mixing in a reservoir at a depth of 3–9 km.

6. Sustained explosive eruptions have delivered at least 12 pumice falls during the past ca. 50 000 yr. Sub-Plinian pumice falls occurred every 2000 to 4000 yr on average, and ash falls occurred every 500 to 1500 yr on average. The last sub-Plinian explosive episode was at ca. 2300–2050 yr B.P.; it released pumice fall and flow ≤0.7 km³ in volume. The last small events were at A.D. 1440–1470 and produced a volume of $\leq 6 \times 10^6$ m³ of ash fall. Lahars swept down the Río Chili valley and tributaries as recently as in the 1600s. Persistent, high-temperature fumarolic activity is observed today on the plug and on the summit's southeast flank

Thus, considerable hazards remain at Arequipa and Chiguata, where 750 000 people may be affected at least indirectly by (1) thick tephra-fall deposits that could cover the city and its airport, (2) pyroclastic flow and surges that could affect the city suburbs 13 km away from the vent, and (3) debris flow and flas flood induced by rainstorms and snowmelt, as well as rockslide avalanches that

DEPOSITS OF THE AD 1440–1470 EVENT AND OF THE ca. 2300–2050 yr B.P. ERUPTIVE EPISODE

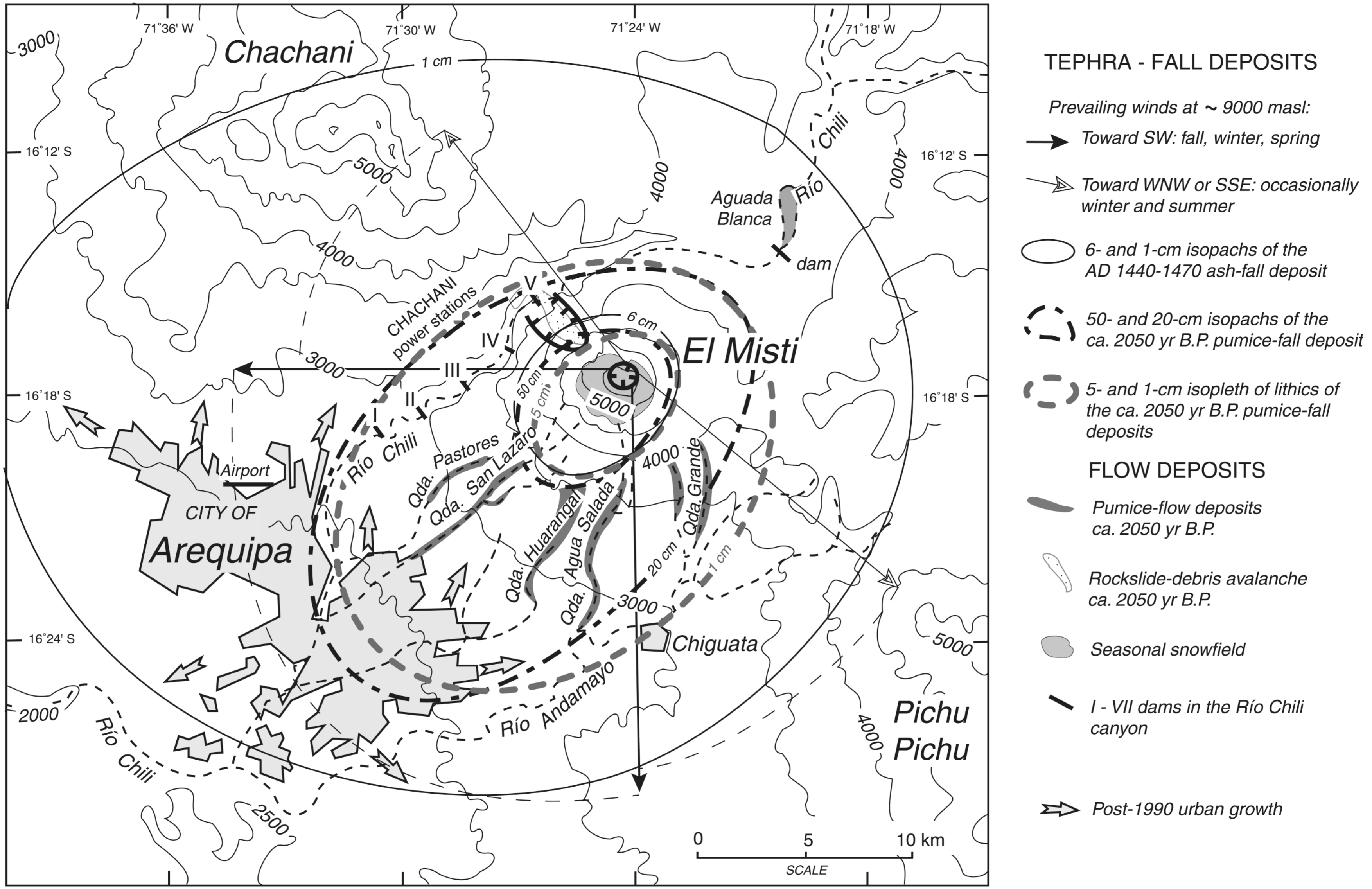

Figure 12. Schematic map showing the 6 and 1 cm isopachs of the A.D. 1440–1470 ash-fall deposit as well as the 50 and 20 cm isopachs and the 5 and 1 cm isopleths of the 2300–2050 yr B.P. pumice-fall deposit. The extent of the pumice-flo deposits is also shown.

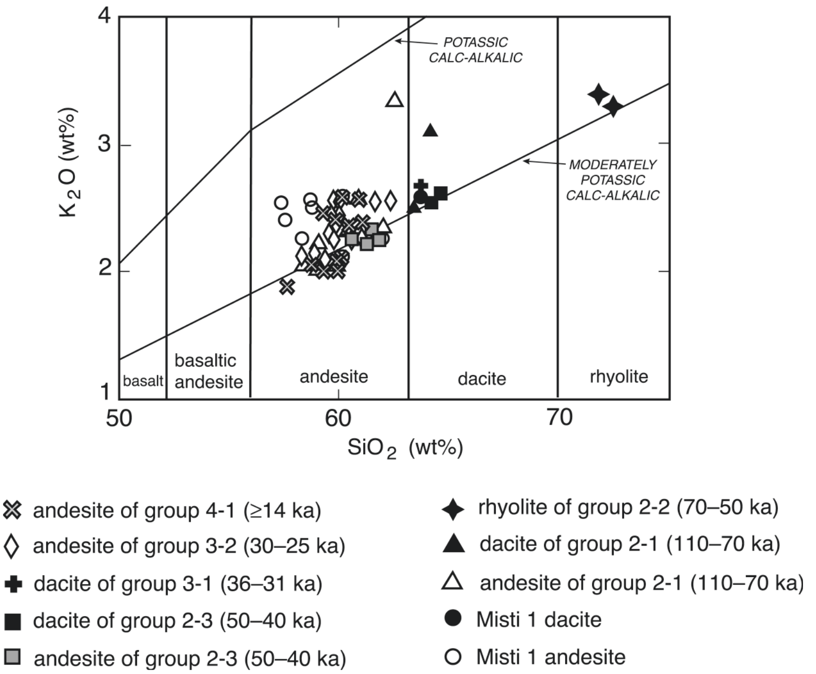

Figure 13. K_2O vs. SiO_2 plot showing the composition of rocks of the groups 2–1 to 4–1 of Misti 2–4 (after Legendre, 1999).

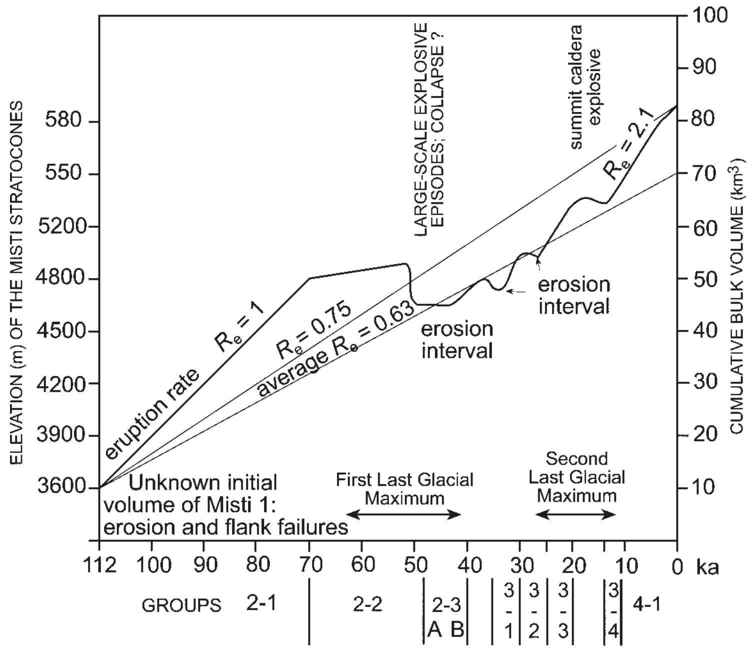

Figure 14. Schematic cumulative eruption volume vs. time for the Misti stratocones 2–4 based on maximum (~83 km³) and minimum (~70 km³) volumes and on edific elevation during the 112-k.y.-long eruptive period. (Volumes are based on the equation 1/3 r^2h, where h = 2.2 km and r = 6–5.5 km.) Minimum and maximum cumulative eruption rates in km³/k.y. and reconstructed curve of growth of the stratocones are also drawn.

could damage the valleys of Río Chili and tributaries.

The possible impact of Misti on Arequipa is as worrisome as that of Vesuvius near Napoli. Poor, densely populated suburbs have spread upstream beyond the 1991 city boundary toward the volcano and the town of Chiguata, the areas most affected by El Misti in recent history (Fig. 12). The lack of emergency-response policy and the lack of land-use planning prevent decision makers from regulating city growth. Future growth of the city should be preferentially oriented southeast and west of the depression but beyond 25 km from the vent.

ACKNOWLEDGMENTS

This research has been supported by the Institut de Recherche pour le Développement during a cooperative research project with the Instituto Geofísico del Perú (IGP) and UMR 6524-CNRS, Université Blaise-Pascal, Clermont-Ferrand. We appreciate the support of IGP (R. Woodman, H. Montes) and Civil Defense in Arequipa (A. Arguedas). We thank J.-Ph. Eissen, O. Macedo, Ch. Legendre, P. Navarro, M. Rivera, J. Dávila, D. Ramos, and R. Gusset for help in fiel and laboratory. We are indebted to J. Hunt, F. Chambers, and G. Williams-Jones for improving drafts and to R. Waitt and S. de Silva for insightful comments.

REFERENCES CITED

Barker, S.D., 1996, El sillar ocioso: Bulletin of Volcanology, v. 58, p. 317–318.

Barriga, V.M., 1951, Los terremotos en Arequipa (1582–1868): Arequipa, La Colmena, 426 p.

Chávez Chávez, J.A., 1992, La erupción del volcán Misti, Pasado, presente, futuro: Arequipa, Impresiones Zenit, 158 p.

Davidson, J., and de Silva, S., 2000, Composite volcanoes, *in* Sigurdsson, H., et al., eds., Encyclopedia of volcanoes: San Diego, Academic Press, 1417 p.

de Silva, S.L., and Francis, P.W., 1991, Volcanoes of the Central Andes: Berlin, Springer, 216 p.

García-Zuñiga, F.F., and Parrot, J.F., 1998, Analyse tomo-morphométrique d'un édific volcanique récent: Misti, Pérou: Paris, Comptes Rendus de l'Académie des Sciences, Sér IIa, v. 327, p. 457–462 (with abridged English version).

Glicken, H.X., 1991, Facies architecture of large volcanic-debris avalanches: Sedimentation in volcanic settings, *in* Fisher, R.V., and Smith, G.A., eds., Sedimentation in volcanic settings: SEPM (Society for Sedimentary Geology) Special Publication 45, p. 99–106.

Hantke, G., and Parodi, A., 1966, Catalogue of the active volcanoes of the world. Part XIX: Colombia, Ecuador and Peru: Naples, IAVCEI, 73 p.

INEI-ORSTOM, 1998, El Perú en Mapas, Atlas en base al censo de población y vivienda: Lima, Institut de Recherche pour le Développement, 140 p.

Jackson, D.B., and Kauahikaua, J., 1987, Regional self-potential anomalies at Kilauea volcano, *in* Decker, R.W., Wright, T.L., and Stauffer, P.H., eds., Volcanism in Hawaii: U.S. Geological Survey Professional Paper 1350, p. 947–959.

Jacquemin, H., and Joron, J.L., 1984, Volcanologie et magmatologie du volcan calco-alcalin El Misti: Paris, Société Géologique de France, Résumé, Tenth Réunion Annuelle des Sciences de la Terre, Bordeaux, p. 300.

Juvigné, E., Thouret, J.-C., Gilot, E., Gourgaud, A., Legros, F., Uribe, M., and Graf, K., 1997, Etude téphrostrati-

graphique et bioclimatique du Tardiglaciaire et de l'Holocène de la Laguna Salinas, Pérou méridional: Géographie Physique et Quaternaire, v. 51, p. 219–231.
Kaneoka, I., and Guevara, C., 1984, K-Ar age determinations of late-Tertiary and Quaternary Andean volcanic rocks, southern Peru: Geochemical Journal, v. 18, p. 233–239.
Lefèvre, C., 1979, Un exemple de volcanisme de marge active dans les Andes du Pérou (sud) du Miocène à l'actuel [Ph.D. thesis]: Montpellier, Université Sciences et Techniques du Languedoc, 555 p.
Legendre, C., 1999, Pétrogenèse du volcan ''Misti moderne'' (Sud Pérou): Essai de caractérisation de l'évolution pétro-géochimique et chronologique: Cergy-Pontoise, Institut de Géologie A Lapparent, Rapport stage fi d'étude, 88 p + annexes.
Legros, F., 1998, Téphrostratigraphie du volcan Misti (Pérou) et modélisation des écoulements pyroclastiques [Ph.D. thesis]: Clermont-Ferrand, France, Université Blaise-Pascal, 150 p.
Macedo, L.F., 1994, Peligro volcánico potencial del Misti [M.Sc. thesis]: Arequipa, Universidad Nacional San Agustín, Convenio DHA-UNDRO-UNSA, 112 p.
Poupeau, G., 1996, *in* Vatin-Pérignon, N., Poupeau, G., Oliver, R.A., Lavenu, A., Labrin, E., Keller, F., and Bellot-Gurlet, L., 1996, Trace and rare-earth element characteristics of acidic tuffs from southern Peru and northern Bolivia and a fission-trac age for the Sillar of Arequipa: Journal of South American Earth Sciences, v. 9, no. 1–2, p. 91–109.
Seltzer, G.O., 1990, Recent glacial history and paleoclimate of the Peruvian-Bolivian Andes: Quaternary Science Reviews, v. 9, p. 137–152.
Seltzer, G.O., Baker, P., Cross, S., Dunbar, R., and Fritz, S., 1998, High-resolution seismic reflectio profile from Lake Titicaca, Peru-Bolivia: Evidence for Holocene aridity in the tropical Andes: Geology, v. 26, p. 167–170.
Simkin, T., and Siebert, L., 1994, Volcanoes of the world (2nd edition): Washington, D.C., Smithsonian Institution, 349 p.
Suni, J., 1999, Estudio geológico y vulcanológico del volcán Misti y sus alrededores [Ph.D. thesis]: Arequipa, Universidad Nacional San Agustin, Facultad Geología y Minas, 179 p.
Thouret, J.-C., 1999, Assessment of volcanic hazards in the area of Arequipa City, based on the eruptive history of the Misti volcano, southern Peru: Zeitschrift für Geomorphologie, supplement, v. 114, p. 89–112.
Thouret, J.-C., Legros, F., Gourgaud, A., Salas, G., Juvigné, E., Gilot, E., Uribe, M., and Rodriguez, A., 1995, Un exemple de prévision des risques volcaniques au Pérou méridional (région d'Arequipa), fondé sur l'étude de l'activité éruptive récente du strato-volcan El Misti: Paris, Comptes Rendus de l'Académie des Sciences, Sér IIa, v. 320, p. 923–929.
Thouret, J.-C., Suni, J., Eissen, J.-Ph., and Navarro, P., 1999a, Assessment of volcanic hazards in the Arequipa area based on the eruptive history of Misti volcano, southern Peru: Zeitschrift für Geomorphologie, band 114, suppl., p. 89–112.
Thouret, J.-C., Dávila, J., and Eissen, J.-Ph., 1999b, Largest historic explosive eruption in the Andes at Huaynaputina volcano, south Peru: Geology, v. 27, p. 435–438.
Vatin-Pérignon, N., Poupeau, G., Oliver, R.A., Lavenu, A., Labrin, E., Keller, F., and Bellot-Gurlet, L., 1996, Trace and rare-earth element characteristics of acidic tuffs from southern Peru and northern Bolivia and a fission-trac age for the Sillar of Arequipa: Journal of South American Earth Sciences, v. 9, no. 1–2, p. 91–109.
Zablocki, C.J., 1976, Mapping thermal anomalies on an active volcano by the self-potential method, Kilauea, Hawaii: San Francisco, California, Proceedings, Second U.N. Symposium on the Development and Use of Geothermal Resources, May 1975, v. 2, p. 1299–1309.
Zamácola y Jaureguí, J.D., 1804, Apuntes para la historia de Arequipa: Primer festival del libro arequipeño: Arequipa, Edición 1958, 15 p.